

Nonlinear second-order dynamics describe labial constriction trajectories across languages and contexts

Michael C. Stern* & Jason A. Shaw

Department of Linguistics, Yale University

*Corresponding author address: 370 Temple St, New Haven, CT 06511

*Corresponding author email: michael.stern@yale.edu

Acknowledgements: We would like to thank Ben Kramer and Yichen Wang for their work on data collection and processing. Aspects of the data described in this paper were first reported at the third Hanyang International Symposium on Phonetics and Cognitive Sciences of Language (HISPhonCog) and the 20th International Congress of Phonetic Sciences (ICPhS). A preliminary version of the model was presented at the 13th International Seminar on Speech Production (ISSP). We would like to thank audiences at each of these meetings for their feedback.

Declaration of Interests: The authors declare that they have no known competing financial interests or personal relationships that could have appeared to influence the work reported in this paper.

Abstract

We investigate the dynamics of labial constriction trajectories during the production of /b/ and /m/ in English and Mandarin. We find that, across languages and contexts, the ratio of instantaneous displacement to instantaneous velocity generally follows an exponential decay curve from movement onset to movement offset. We formalize this empirical discovery in a differential equation and, in combination with an assumption of point attractor dynamics, derive a nonlinear second-order dynamical system describing labial constriction trajectories. The equation has only two parameters, T and r . T corresponds to the target state and r corresponds to movement rapidity. Thus, each of the parameters corresponds to a phonetically relevant dimension of control. Nonlinear regression demonstrates that the model provides excellent fits to individual movement trajectories. Moreover, trajectories simulated from the model qualitatively match empirical trajectories, and capture key kinematic variables like duration, peak velocity, and time to achieve peak velocity. The model constitutes a proposal for the dynamics of individual articulatory movements, and thus offers a novel foundation from which to understand additional influences on articulatory kinematics like prosody, inter-movement coordination, and stochastic noise.

Keywords: articulatory dynamics, articulatory phonology, articulatory phonetics, dynamical systems

Highlights:

- Ratio of displacement to velocity in lip constrictions follows exponential decay.
- A nonlinear second-order dynamical model derives this observation.
- Model parameters are T (target state) and r (movement rapidity).
- Model provides excellent fits to acceleration as a function of velocity and state.
- Model-generated trajectories capture key measures of articulatory kinematics.

1. Introduction

1.1 Background

Speech articulation involves coordinated movements of articulatory organs like the tongue, lips, and larynx in order to generate sound. These movements can be characterized as dynamical systems: sets of variables which change lawfully over time. The formal expression of a dynamical system is given in Eq. 1:

$$\dot{\mathbf{x}} = \mathbf{f}(\mathbf{x}) \quad (1)$$

\mathbf{x} is the set of variables which characterizes the state of the system at any given time. In speech articulation, this set of variables could in theory be extremely large, e.g., including the three-dimensional spatial position of each articulator, the tension of each muscle relevant for moving the articulators, or even the membrane potential of each neuron relevant for articulatory motor control. In practice, however, speech articulation can be described using a relatively small number of “task” variables which are subserved by flexible synergies of other variables, as in Task Dynamics (Saltzman & Munhall, 1989). In this way, the high-dimensional space of potentially relevant variables is reduced. For instance, *lip aperture* (LA)—the distance between the upper and lower lip—is a task variable relevant for producing labial sounds like /b/ and /m/, which is controlled by a synergy between the positions of the upper lip, lower lip, and jaw.

Eq. 1 describes the time derivatives of \mathbf{x} , i.e., $\dot{\mathbf{x}}$ or the rates of change of \mathbf{x} , as some set of functions $\mathbf{f}(\mathbf{x})$. An important benefit of such a dynamical characterization of speech articulation is that it allows an explicit link between time-variant articulatory trajectories and stable (relatively time-invariant) control parameters, i.e., the coefficients of the terms in $\mathbf{f}(\mathbf{x})$. These control parameters can be interpreted as cognitive representations. For instance, Articulatory Phonology (e.g., Browman & Goldstein, 1989) links control parameters of the functions in Task Dynamics (in particular, “stiffness” k and target position T) to dimensions of phonological contrast in language. In this way, dynamical models bridge the traditional divide between discrete and continuous representations in linguistics (Iskarous, 2017; Iskarous & Pouplier, 2022) and cognitive science more broadly (van Gelder, 1998). In order for the control parameters of $\mathbf{f}(\mathbf{x})$ to be theoretically interpretable, they should be relatively few in number (e.g., Brunton et al., 2016). Moreover, articulatory trajectories simulated by $\mathbf{f}(\mathbf{x})$ should be qualitatively similar to real articulatory trajectories under a variety of conditions, e.g., variation in linguistic prosody (e.g., Byrd & Saltzman, 1998, 2003) or mechanical perturbation of the articulators (e.g., Abbs & Gracco, 1984).

A useful kind of dynamical system for modeling speech articulation (as well as other kinds of goal-directed behavior) is a *point attractor*, as in Eq. 2.¹

$$\lambda \dot{x} = -x + T \quad (2)$$

The system described by Eq. 2 has a point attractor because \dot{x} is negatively related to x . Regardless of the particular value of x at any given time, \dot{x} will be in the direction of T , i.e., x will be moving towards T . Moreover, when $x = T$, $\dot{x} = 0$. In other words, x stops moving when x reaches T . For this reason, T is the point attractor of the system, called T in this case for “target” (cf. Mücke et al., 2024). Moreover, the magnitude of \dot{x} at any given time is proportional to the difference between x and T at that time, as well as the control parameter λ . In other words, the farther away x is from T , the more quickly x moves towards T , with the actual magnitude modulated by λ . This captures an important fact about speech articulation, namely that the peak velocity of a movement is robustly correlated with total movement amplitude (Ostry & Munhall, 1985). The farther an articulator travels to reach its target, the faster it moves.

Speech articulation can be characterized as a sequence of target-directed movements governed by point attractor dynamics. For instance, articulating /b/ requires bringing the lips together to form a closure. In this case, x is lip aperture (LA), λ controls the rate of movement, and T is either zero, indicating that the lips are together, or a small negative number, indicating a target just beyond what is physically possible (e.g., Parrell, 2011). In this way, Eq. 2 captures the basic target-directedness of articulatory movement, with differences between movements arising from variation in the positions of the targets and in the speeds of the movements. However, the shapes of the trajectories generated by Eq. 2 are quite different from observed trajectories. In particular, for any fixed value of the control parameter λ , simulated trajectories achieve peak velocity instantaneously; velocity then decreases monotonically as x approaches T . In real trajectories, peak velocity occurs later, approximately halfway through the movement (Ostry et al., 1987). The observed delay in the achievement of peak velocity has inspired the use of a *damped mass-spring* model of speech articulation, as in Eq. 3:

$$b\dot{x} = k(-x + T) - m\ddot{x} \quad (3)$$

In Eq. 3, peak velocity is delayed (relative to Eq. 2) because velocity \dot{x} is negatively related to acceleration \ddot{x} . This empirical improvement is achieved via greater model complexity: Eq. 3 is a second-order system, referencing the second time derivative \ddot{x} or acceleration, unlike the first-order system in Eq. 2, which only

¹ Henceforth we focus on the dynamics of individual variables, hence the unbolded symbols.

references the first time derivative \dot{x} or velocity. Moreover, Eq. 3 has four control parameters m , b , k , and T , more than the two parameters λ and T in Eq. 2.²

Even in the second-order model in Eq. 3, however, peak velocity occurs unrealistically early (Perrier et al., 1988). Thus, more complexity has been added to Eq. 3. One approach has been to add a time-varying activation parameter $a(t)$ (Byrd & Saltzman, 1998; Kröger et al., 1995). Allowing $a(t)$ to ramp up over time successfully delays the achievement of peak velocity, more closely matching empirical velocity trajectories. Another approach has been to add a cubic term $d(-x + T)^3$ (Sorensen & Gafos, 2016). This delays the achievement of peak velocity by reducing acceleration at large distances from the target. This approach also captures non-linearity in the relationship between peak velocity and total movement amplitude (Ostry & Munhall, 1985). Both of these approaches achieve greater empirical adequacy, but at a cost. The first approach introduces a dependence on time t , making the system *non-autonomous*, which has been argued to be undesirable for dynamical models of behavior (Fowler, 1980; Sorensen & Gafos, 2016). The second approach preserves autonomy, but only by introducing an additional parameter d , increasing model complexity and reducing the theoretical interpretability of each parameter.³

1.2 Empirical bases of existing dynamical models

In this subsection we summarize the data that has informed the existing dynamical models of articulation described in Section 1.1, in order to better situate the data reported in the present study. One of the first applications of the damped mass-spring model to speech articulation was from Ostry & Munhall (1985), who adapted the idea from research on limb movements (Cooke, 1980). Ostry & Munhall (1985) used ultrasound imaging to measure tongue dorsum kinematics during repetition of CV syllables from three speakers of Canadian English. They found a robust correlation between the maximum spatial displacement of a movement and its peak velocity in all three speakers, which is well-captured by the damped mass-spring model. They also proposed that the model's stiffness parameter k is involved in controlling speech rate. Kröger et al. (1995) enriched the damped mass-spring model by introducing continuous activation ramping and de-ramping at the beginning and end of movements, respectively. They used electromagnetic articulography (EMA) to track lip, tongue tip, and tongue body movements of three native speakers of German during production of CV syllables which were parts of real words in carrier phrases. Addition of

² Some implementations of the damped mass-spring model constrain certain parameters so that there are functionally fewer than four free parameters.

³ Another theoretical approach that improves model fits to articulatory data relative to the original damped mass-spring model is General Tau theory (Lee, 1998), as developed in Elie et al. (2023, 2024). General Tau theory describes point attractor dynamics that are both non-autonomous and non-linear, and require reference to the temporal duration of the movement. This last feature brings it beyond the incremental theoretical development pursued in this paper.

the activation-ramping mechanism was largely motivated by symmetrical velocity shapes, which cannot be generated by the original damped mass-spring model. For similar reasons, Byrd & Saltzman (1998) also used activation ramping in their implementation of the damped mass-spring model. Their data came from EMA recordings of lip movements in three speakers of English producing sentences with target words in varying prosodic contexts. They found that prosodic variation could be captured through a combination of variation in stiffness k and variation in parameters controlling the shape of the activation curve. Sorensen & Gafos (2016) replaced activation ramping with a cubic term in order to eliminate explicit dependence on time and therefore preserve system autonomy. They analyzed two sets of data: one dataset consisting of x-ray microbeam (XRMB) recordings of tongue dorsum movements from 43 English speakers producing isolated nonwords, and another consisting of EMA recordings of lip movements from three English speakers producing repeated CV syllables. They found that the damped mass-spring model with an additional cubic term could generate the observed symmetrical velocity trajectories and cubic-shaped Hooke diagrams (acceleration by displacement) without the need for time-dependent activation ramping. Finally, Kuberski & Gafos (2023) evaluated fits of the original damped mass-spring model to EMA recordings of tongue tip and tongue body movements during repetition of CV syllables at different metronome rates in five speakers of English and five speakers of German. They found that, in general, fits were better at faster rates and with more aggressive thresholding for the measurement of movement onsets and offsets, reflecting the fact that the relationship between acceleration and position is less linear at greater spatial displacement. The five studies are summarized in Table 1.

Study	Subjects	Measurement	Articulator(s)	Speech type
Ostry & Munhall (1985)	3	Ultrasound	Tongue dorsum	Repeated syllables
Kröger et al. (1995)	3	EMA	Lips, tongue tip, tongue body	Words in carrier phrases
Byrd & Saltzman (1998)	3	EMA	Lips	Sentences with varying prosody
Sorensen & Gafos (2016)	46	XRMB, EMA	Tongue dorsum, lips	Isolated nonwords, repeated syllables
Kuberski & Gafos (2023)	10	EMA	Tongue tip, tongue body	Repeated syllables

Table 1: Summary of data types informing existing dynamical models of speech articulation.

Each of these studies has provided invaluable insights into the nature of articulatory dynamics. However, small numbers of subjects and/or non-naturalistic speech types, e.g., syllable repetition or isolated nonwords, necessitates care in generalizing the results across individuals, languages, and speech contexts. One of the goals of the present study is to extend the body of data bearing on speech articulatory dynamics

by examining a relatively large number of subjects (24) producing meaningful sentences in two unrelated languages (English and Mandarin).

1.3 This study

In this study, we contribute to the goal of uncovering the basic dynamics of articulatory movements, with a focus on balancing model simplicity and empirical adequacy. Rather than starting from the specific second-order system in Eq. 3, we start from a minimal assumption of point attractor dynamics, formalized in Eq. 2. This allows us to solve for the parameter λ from measurement of data, in particular, electromagnetic articulography (EMA) recordings of bilabial constriction movements during the production of /b/ and /m/ in CV sequences in English and Mandarin speakers. In this way, we address the question: what is the empirical relationship between velocity \dot{x} and state x over time? The answer to this question guides dynamical model development. We focus on bilabial movements because the hypothesized task dimension of lip aperture (LA) is transparently related to the measurable spatial positions of the upper and lower lips (via the Euclidean distance). In contrast, task dimensions governing tongue movements, i.e., constriction location and constriction degree, are not as transparently related to measurable spatial positions of fleshpoints on the tongue. Moreover, we focus on the constriction phase of the movement (cf. Kuberski & Gafos, 2023), rather than the release phase, because there is evidence that the dynamics of the release phase are coupled to the following vowel constriction movement (Kramer et al., 2023). This coupling would introduce additional complexity into the kinematics of the movement. Thus, labial constriction movements present an ideal test case for uncovering the dynamics of individual articulatory movements.

2. Experimental methods

2.1 Data availability

The data, analysis code, and simulation code for generating the results reported below are available on OSF at <https://osf.io/7f2mh/>.

2.2 Participants

Data was collected from 24 subjects: 12 native speakers of American English (8 female, 4 male, ages 19–28, mean = 20.75) and 12 native speakers of Mandarin Chinese (7 female, 4 male, 1 nonbinary, ages 19–33, mean = 24.00). All participants self-reported no history of speech, language, or hearing impairment.

2.3 Materials

Stimuli consisted of eight word-initial CV sequences in each language, where the initial consonant was bilabial—either [b] or [m]—and the vowel was either low back [ɑ] or high front [i]. Target sequences containing the vowel [i] were immediately preceded by the vowel [ɑ], and sequences containing the vowel [ɑ] were immediately preceded by the vowel [i]. All Mandarin target syllables bore a falling tone (T4) and were preceded immediately by a low tone (T3). Each target syllable was produced in two carrier sentences, occurring once in an informationally prominent position and once in a less prominent position. To encourage natural speech, each carrier sentence was preceded by a question, which served to provide context for the target sentences. Examples of context questions and target carrier sentences are given in Table 2.

Item	Language	Prominence	Stimulus	
[i _{ma}]	English	Not prominent	Prompt	Is she a knee model client?
			Target	She’s a knee <u>model</u> representative , not a knee model client.
		Prominent	Prompt	Is she a knee surgeon?
			Target	She’s a knee model , not a knee surgeon.
	Mandarin	Not prominent	Prompt	Wo3 ying1gai1 ma4 ta1 hai2shi4 ma4 ni3? ‘Should I scold him or scold you?’
			Target	Ni3 <u>ma4 ta1</u> jiu4 xing2 le0, bie2 ma4 wo3. ‘Just scold him; don’t scold me.’
		Prominent	Prompt	Wo3 ying1gai1 ma4 ta1 hai2shi4 da3 ta1? ‘Should I scold him or hit him?’
			Target	Ni3 ma4 ta1 jiu4 xing2 le0, bie2 da3 ta1. ‘Just scold him; don’t hit him.’

Table 2: Example stimuli. Target CV sequences are underlined; prominent words are bolded.

2.4 Procedure

Presentation of materials was controlled using E-Prime. On each trial, an audio recording of a question was played. The question was also displayed in text on the screen for 5000 ms. Participants were instructed to listen to the question and to read aloud the answer that followed. In total, each participant produced 128 tokens (8 items \times 2 carrier sentences \times 8 repetitions) across four blocks of 32 items each. Within each block, stimuli were presented in a randomized order.

Articulatory kinematic data was collected with the NDI Wave Speech Research System sampling at a rate of 100 Hz. The sensors of interest for this study were attached at the vermilion border of the upper lip (UL) and lower lip (LL). Three sensors were also attached to the tongue: tongue tip (TT), tongue blade (TB), and tongue dorsum (TD), placed \sim 1 cm, \sim 3 cm, and \sim 5 cm from the tip of the tongue, respectively. In order to track movements of the jaw, one lower incisor (LI) sensor was attached to the hard tissue of the gum directly below the left incisor. Reference sensors were attached on the left and right mastoids and on the nasion. Measurements of the occlusal plane and a midsagittal palate trace were also collected. Acoustic data was collected using a Sennheiser shotgun microphone at a sampling rate of 22,050 Hz.

2.5 Data processing

Articulatory data was rotated to the occlusal plane and corrected for head movement computationally. Trajectories were smoothed using the robust smoothing algorithm of Garcia (2010). First and second time derivatives (velocity and acceleration) were calculated from the smoothed trajectory using central differencing, then lowpass filtered using a 5th order Butterworth filter. Consonant constriction movements were parsed from the lip aperture (LA) signal, calculated as the Euclidean distance between the UL and LL sensors. The onset and offset of each movement were marked as the timepoints at which velocity exceeded or fell below, respectively, a 20% threshold of peak velocity, manually selected in MVIEW (Tiede, 2005). For the calculation of displacement, the spatial target of each movement (i.e., T) was defined as the LA value at the timepoint of minimum velocity following movement offset (recall that at movement offset, velocity is still at 20% of the peak). Using this measure of movement target T , we calculated displacement at each sample as the difference between the target and the current state of LA, i.e., $T - x$ (or alternatively, $-x + T$ as in Eq. 2).

λ was calculated at each sample as the ratio of instantaneous displacement to instantaneous velocity: $(-x + T)/\dot{x}$ (see Eq. 2). By demarcating movements based on a 20% threshold of peak velocity, instead of, e.g., velocity zero-crossing, we exclude portions of the kinematics in which displacement or velocity

are infinitesimal. This prevents λ from approaching 0 (infinitesimal displacement) or infinity (infinitesimal velocity). Movement duration was calculated by subtracting the timestamp of the onset of movement from the timestamp of the offset of movement. We also calculated a measure of “kinematic stiffness” for each movement by dividing peak velocity by maximum displacement (e.g., Roon et al., 2021). In this dataset, maximum displacement was always onset state minus target state. In order to plot trajectories together, all trajectories were upsampled to 100 samples using shape-preserving cubic Hermite interpolation.

Out of the 3072 tokens elicited, a total of 962 tokens (31.3%) were eliminated from analysis for the following reasons: failure of the parsing tool to extract the movement (447 tokens); a non-monotonic trajectory, i.e., instantaneous velocity changed sign for at least one sample (306 tokens); failure of the participant to produce contrastive focus on the informationally prominent syllable, as judged by a research assistant (155 tokens); disfluency (5 tokens); or data storage failure (49 tokens). 2110 tokens, all of which involved monotonic decreases in displacement, entered the analysis.

3. Experiment results

3.1 Kinematics

Figure 1 displays average trajectories of displacement (left), velocity (center), and acceleration (right) over time, from movement onset to movement offset.

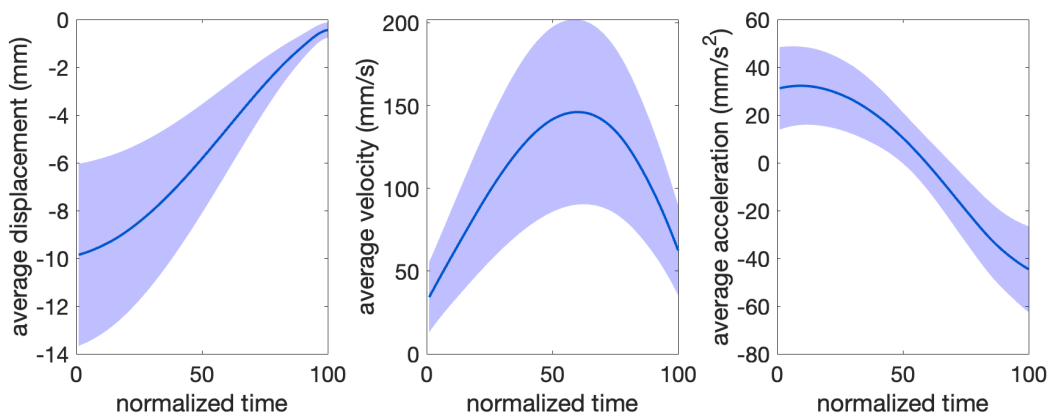


Figure 1: Average trajectories across all tokens ($n = 2110$). Shading indicates one standard deviation.

It can be seen that displacement follows a sigmoidal shape, corresponding to a parabolic shape in the velocity curve and a cubic shape in the acceleration curve. Figure 2 displays the distributions of the

kinematic variables, duration, maximum displacement, kinematic stiffness, peak velocity, absolute time to peak velocity, and relative time to peak velocity (as a ratio of movement duration), across all 2110 tokens from all 24 speakers.

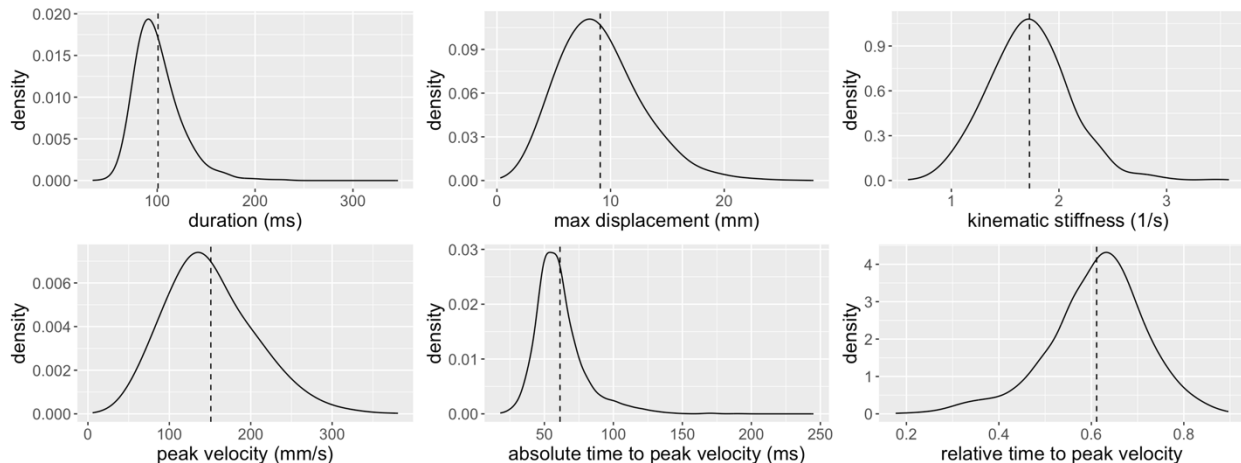


Figure 2: Distributions of kinematic variables across all tokens ($n = 2110$). Dashed vertical lines indicate the mean.

Mean movement duration was 100.86 ms, and the distribution of measurements had a long rightward tail (Figure 2: top left). The distribution of the other durational measure, absolute time to peak velocity, also had a long rightward tail, with a mean of 61.32 ms (Figure 2: bottom center). The other distributions are more normal. The average trajectories in Figure 1 and the distributions of kinematic variables in Figure 2 provide two distinct but related perspectives on the data. Consider the timing of the peak in the average velocity curve in Figure 1 in tandem with the distribution of relative time to peak velocity values in Figure 2. The peak in the average velocity curve is at 0.6 of total movement duration. Correspondingly, mean relative time to peak velocity across all movements was 0.61. Thus, on average, the velocity curves in this dataset are almost symmetric but slightly left-skewed, with peak velocity tending to occur slightly later than halfway through the movement.

3.2 λ trajectories

Next we examine the trajectories of λ , i.e., the ratio of instantaneous displacement to instantaneous velocity. As seen in Figure 3 (top), regardless of language and vowel context, λ generally followed an exponential

decay curve from movement onset to offset. Consistent with this observation, the natural log of λ , henceforth $\ln(\lambda)$, follows an approximately linear trend (Figure 3: bottom).

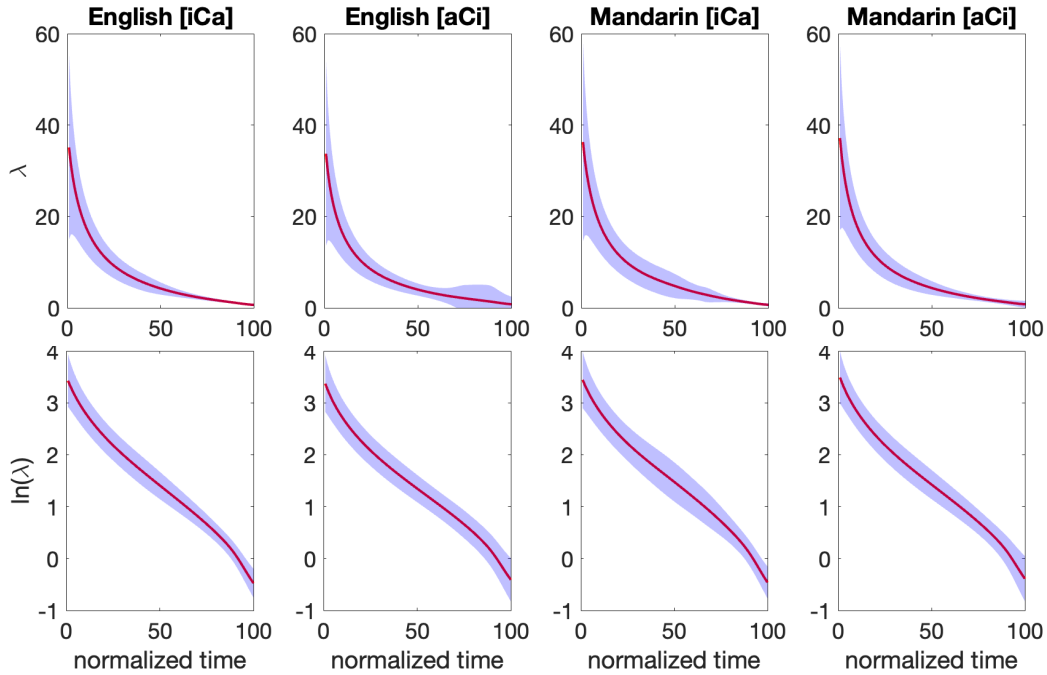


Figure 3: Average trajectories of λ (top) and $\ln(\lambda)$ (bottom) by language and vowel context. The mean is shown in red with one standard deviation in blue. In these plots, 44 tokens (2.1%) were removed which had extremely large initial λ values ($\lambda_0 > 150$; these tokens are still included in all analyses).

To evaluate the robustness of this generalization, a linear regression model was fit to each trajectory of $\ln(\lambda)$ over time. The fits were excellent: overall mean $R^2 = .97$. Moreover, as seen in Figure 4, the slope of each linear fit correlates strongly with linguistically relevant measures like movement duration (Spearman's $\rho = .83$, $p < .001$) and kinematic stiffness ($\rho = -.82$, $p < .001$). Steeper (more negative) slopes correspond with decreased duration and increased kinematic stiffness.

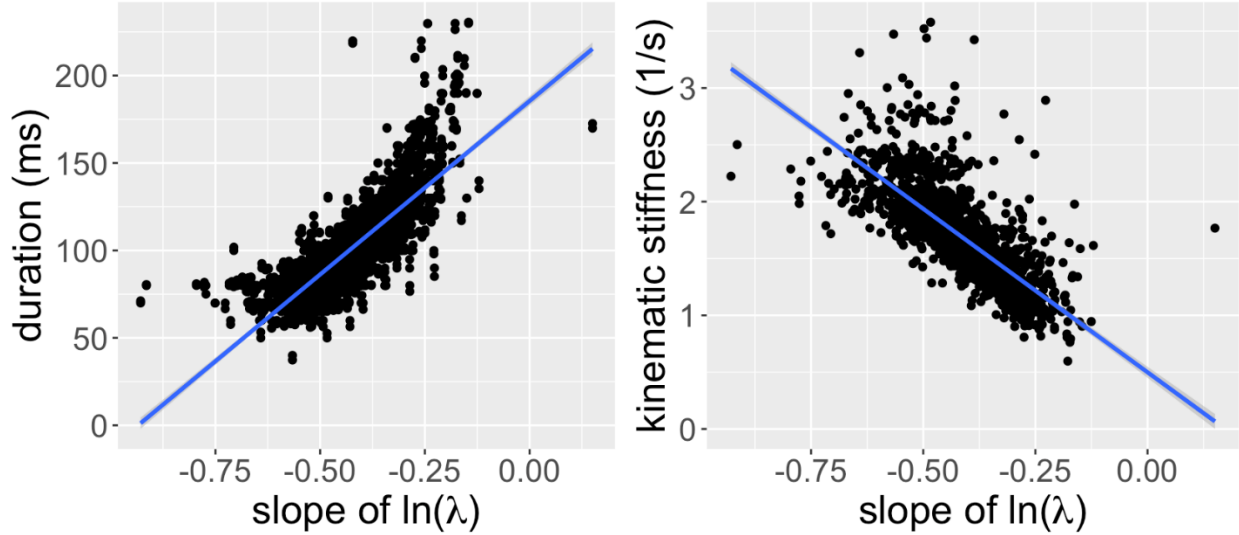


Figure 4: Correlations between the slope of a regression line fit to $\ln(\lambda)$ and two kinematic variables: movement duration (left) and kinematic stiffness (right).

4. Gestural model

4.1 Formalization

The empirical observation of exponential decay in λ over time can be expressed as a differential equation as in Eq. 4, with r controlling the rate of decay. We call this parameter r because the rate of decay in λ corresponds to the “rapidity” of movement, as seen in Figure 4. Higher values of r correspond to shorter duration (Figure 4: left) and higher kinematic stiffness (Figure 4: right).

$$\dot{\lambda} = -r\lambda \quad (4)$$

Together, the two first-order equations in Eq. 2 and Eq. 4 express a dynamical system of two variables, x and λ . Since λ is defined in Eq. 2 as $(-x + T)/\dot{x}$, we can substitute this definition into Eq. 4 to derive a single second-order equation, eliminating λ . This equation, solved for acceleration \ddot{x} , is shown in Eq. 5. See Appendix A for the full derivation.

$$\ddot{x} = r\dot{x} - \dot{x}^2/(-x + T) \quad (5)$$

Eq. 5 has only two parameters, T and r , which can both be inferred from data and have clear interpretations. T corresponds to the spatial target, and r corresponds to movement rapidity, similar to stiffness k in the damped mass-spring model. Moreover, the system is autonomous as it does not reference time (Fowler, 1980; Sorensen & Gafos, 2016). Unlike the linear damped mass-spring model, the system in Eq. 5 is nonlinear, as seen in the second term in the right side of the equation. This issue is discussed further in Section 5.

4.2 Model fitting

We fit the parameters T and r in Eq. 5 to each acceleration \ddot{x} curve as a function of state x and velocity \dot{x} using non-linear least squares regression. The distribution of R^2 values (indicating the goodness of fit) across the 2110 tokens is displayed in Figure 4.

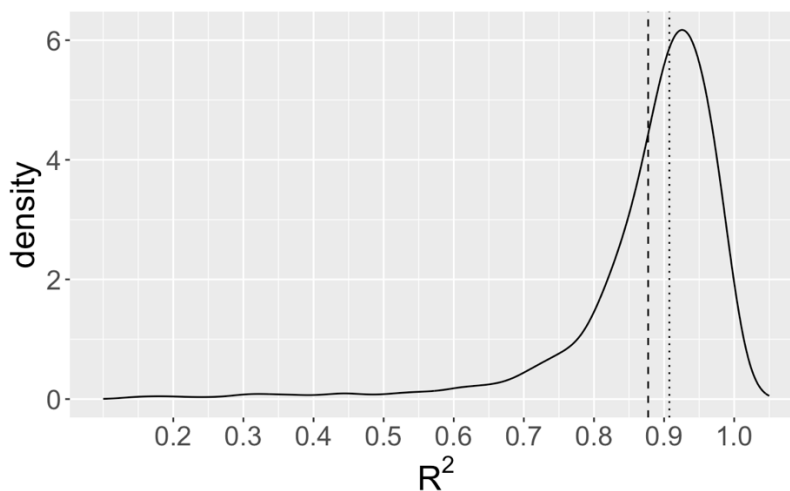


Figure 5: Distribution of R^2 values across 2110 fitted tokens. The dashed line indicates the mean (0.88); the dotted line indicates the median (0.91).

As seen in Figure 5, the fit of the model is generally excellent, with mean $R^2 = 0.88$ and median $R^2 = 0.91$. There are some outlier tokens with poorer fits, as seen in the leftward skew in the distribution. Of the 2110 analyzed tokens, 73 tokens have R^2 values below 0.6. 47 of these tokens have multiple velocity peaks, i.e., acceleration crosses zero multiple times. The other 26 tokens have additional bends in the velocity trajectory; i.e., acceleration approaches zero multiple times. Figure 6 displays example Hooke planes (acceleration by state) for a well-fit token ($R^2 = 0.99$; left) and a poorly fit token ($R^2 = 0.31$; right). It can be seen that the poorly fit token (Figure 6: right) has multiple zero-crossings in the acceleration curve, while

the corresponding model-generated curve has only a single zero-crossing. In Section 5 we discuss potential sources of abnormal trajectories and the failure of the model to fit them well.

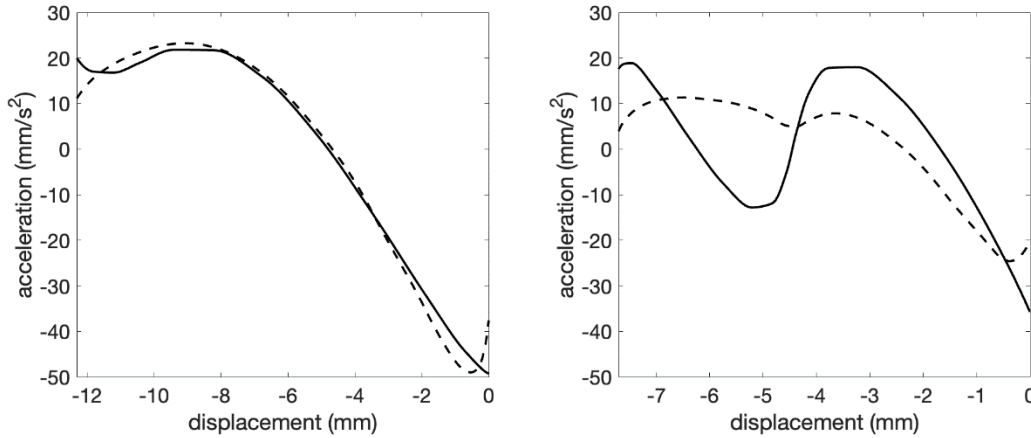


Figure 6: Hooke planes (acceleration by state) for a well-fit token ($R^2 = 0.99$; left) and a poorly fit token ($R^2 = 0.31$; right). Observed acceleration curves are solid; model-generated curves are dashed.

Figure 7 displays the distributions of the values of the parameters r and T fit to each trajectory.

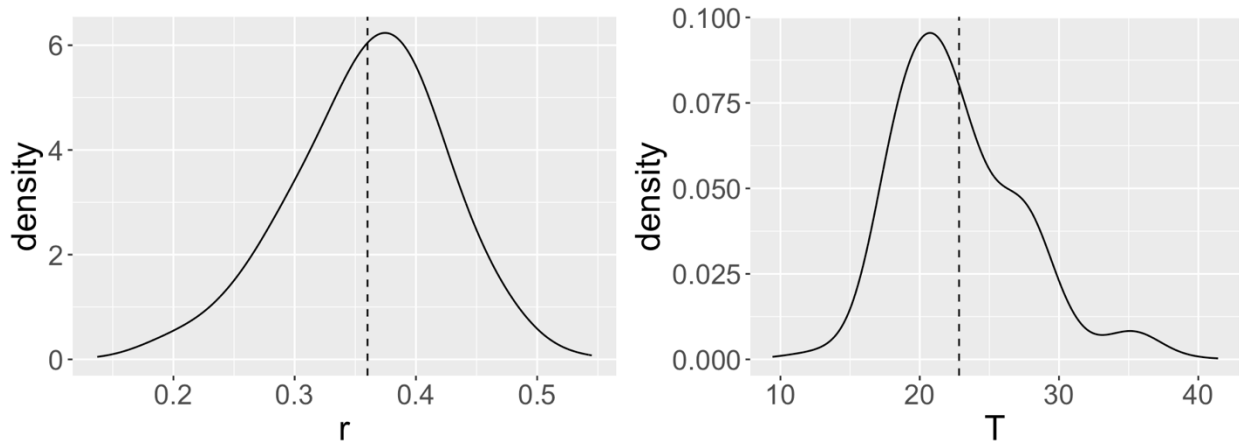


Figure 7: Distributions of fitted values for the parameters r (left; $M = 0.36$, $SD = 0.06$) and T (right; $M = 22.82$, $SD = 4.60$).

The fitted values of r correlate strongly with the slopes of the regression lines fit to $\ln(\lambda)$ ($\rho = -.94$, $p < .001$; Figure 8, left), and the fitted values of T correlate strongly with LA state at the timepoint of minimum velocity ($\rho = 1$, $p < .001$; Figure 8, right). Interestingly, fitted T values tend to be smaller (more constricted

lips; mean = 22.82) than observed final LA states (mean = 23.44), suggesting a pattern of target undershoot (e.g., Lindblom, 1963; Moon & Lindblom, 1994).

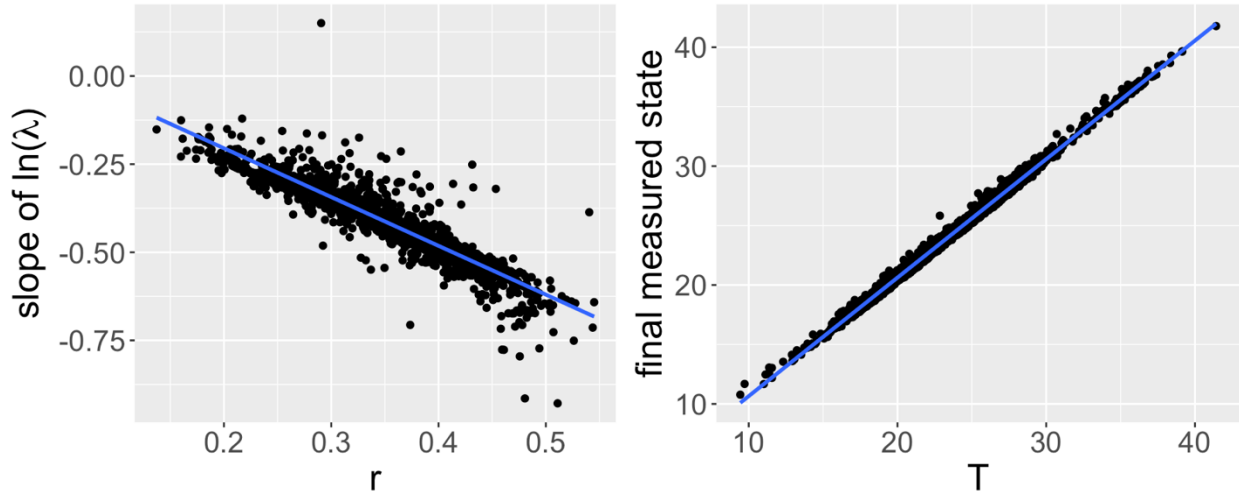


Figure 8: Relationship between fitted parameter values (x -axes) and corresponding measured values (y -axes).

4.3 Model simulation

Another way to evaluate the model is to generate trajectories from Eq. 5 using the fitted values of the control parameters r and T . Then, generated trajectories can be compared to real trajectories. This differs from the approach in Section 4.2 in that only *initial* state and *initial* velocity are considered here; the full trajectories of state, velocity, and acceleration are then generated solely from the model in Eq. 5. In Section 4.2, on the other hand, the entire observed state and velocity trajectories were used to fit the acceleration curve, rather than generating these trajectories from the model.

For each token, we set x_0 and \dot{x}_0 as their observed values, and calculated \ddot{x}_0 from Eq. 5 using the fitted values of r and T . Next, \dot{x}_1 was calculated as $\dot{x}_0 + \ddot{x}_0$, x_1 was calculated as $x_0 + \dot{x}_1$, and \ddot{x}_1 was calculated from \dot{x}_1 , x_1 , r and T using Eq. 5. We iterated this process t times until \dot{x}_t fell below \dot{x}_0 (20% of measured peak velocity). Average simulated trajectories are displayed in Figure 9 (top) with average observed trajectories reproduced for comparison in Figure 9 (bottom).

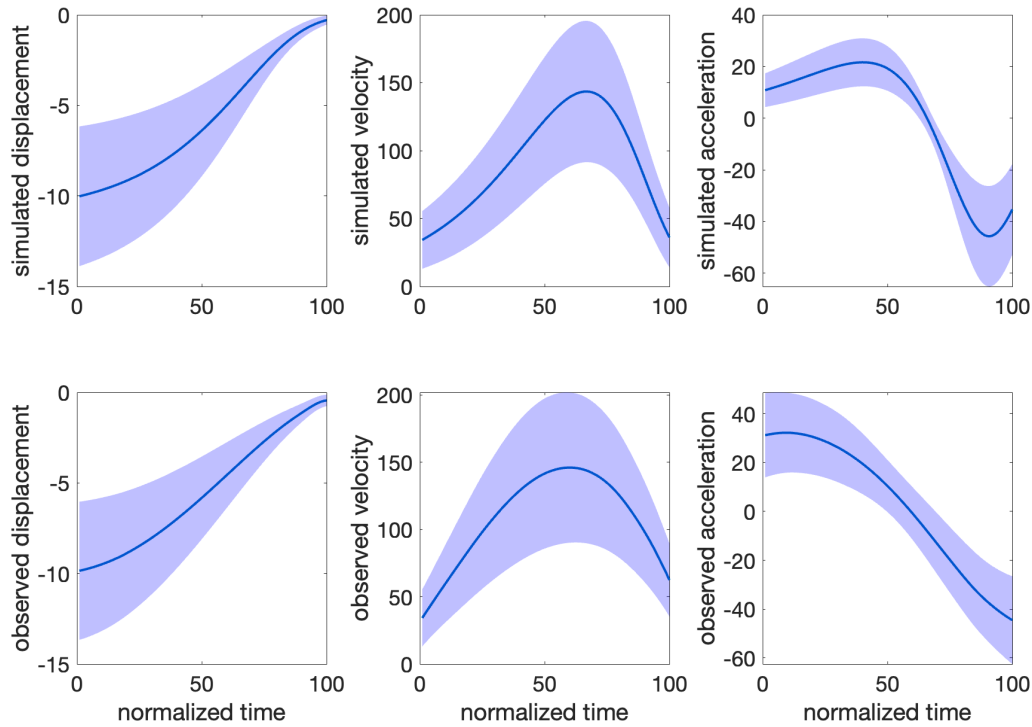


Figure 9: Average trajectories simulated from model fits (top) and observed in the data (bottom).

We calculated R^2 for the fit of each model-generated trajectory (\ddot{x} , \dot{x} , and x) to each corresponding observed trajectory. Overall, model-generated state trajectories x were closest to the observed trajectories (mean $R^2 = 0.93$), followed by acceleration \ddot{x} (mean $R^2 = 0.74$), followed by velocity \dot{x} (mean $R^2 = 0.45$).

In order to further assess the relationship between model-generated and observed trajectories, we measured the same set of kinematic variables as those measured for the observed trajectories and displayed in Figure 2. Figure 10 displays the model-generated distributions.

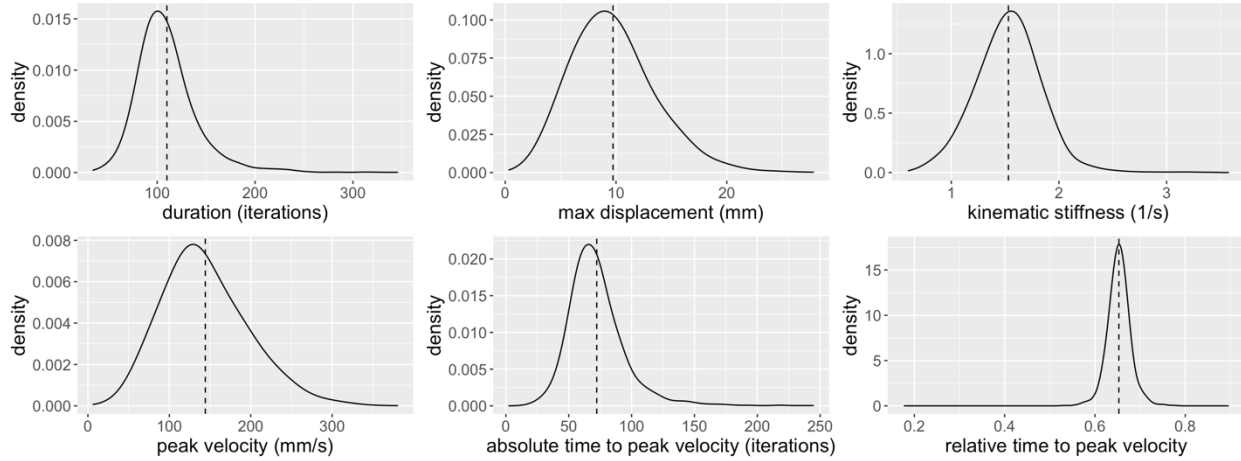


Figure 10: Distributions of kinematic variables measured from simulated trajectories. x -axis limits match those from Figure 2 for comparison.

Next, Figure 11 displays the relationships between the model-simulated kinematic variables and the corresponding observed variables.

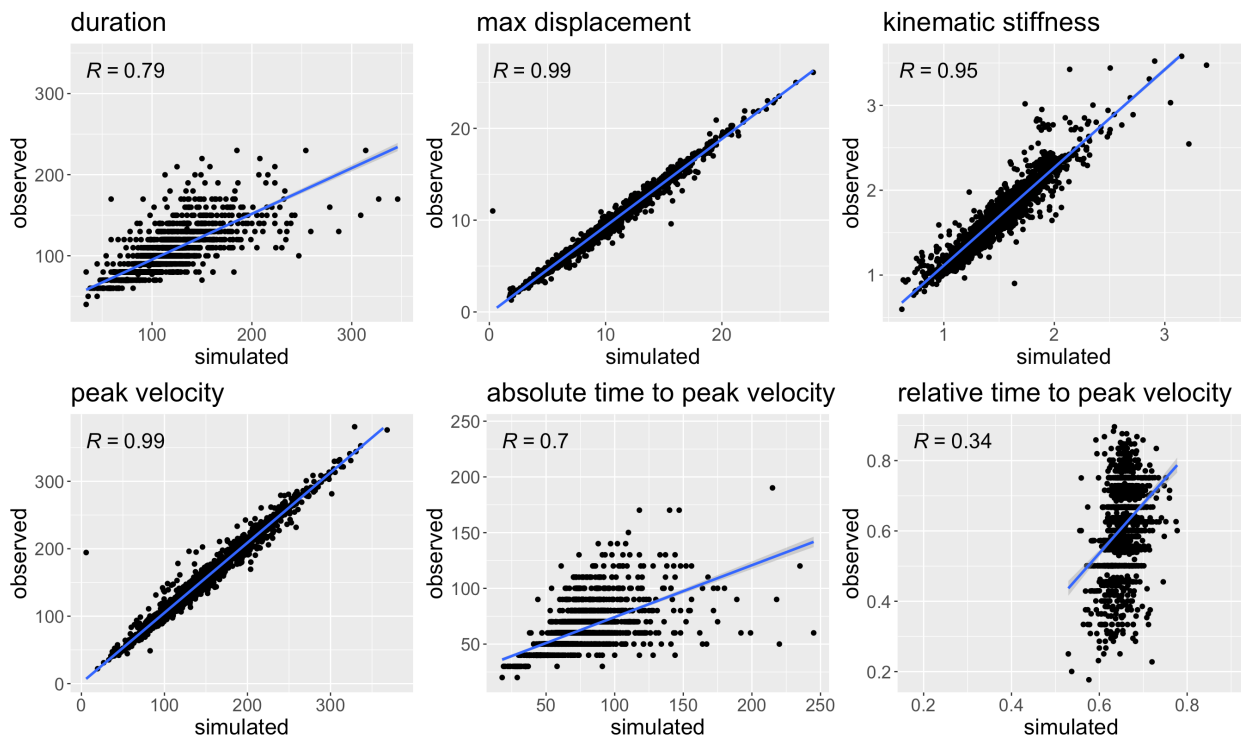


Figure 11: Relationships between model-simulated and observed kinematic variables.

In general, simulated kinematic variables are highly correlated with observed kinematic variables (all p -values $< .001$). The weakest correlation was observed in relative time to peak velocity. Simulated trajectories exhibited very low variation in this variable ($SD = 0.03$) relative to the observed variation ($SD = 0.10$). We revisit this issue in Section 5.

Finally, as seen in Figure 12 (left), model-simulated trajectories replicate the slightly non-linear relationship between maximum displacement and peak velocity observed in both previous datasets (e.g., Ostry & Munhall, 1985) as well as the current dataset (Figure 12: right). Recall that the non-linearity in this relationship was one motivation for the addition of a cubic term to the damped mass-spring model (Sorensen & Gafos, 2016). Our model captures this fact without additional control parameters.

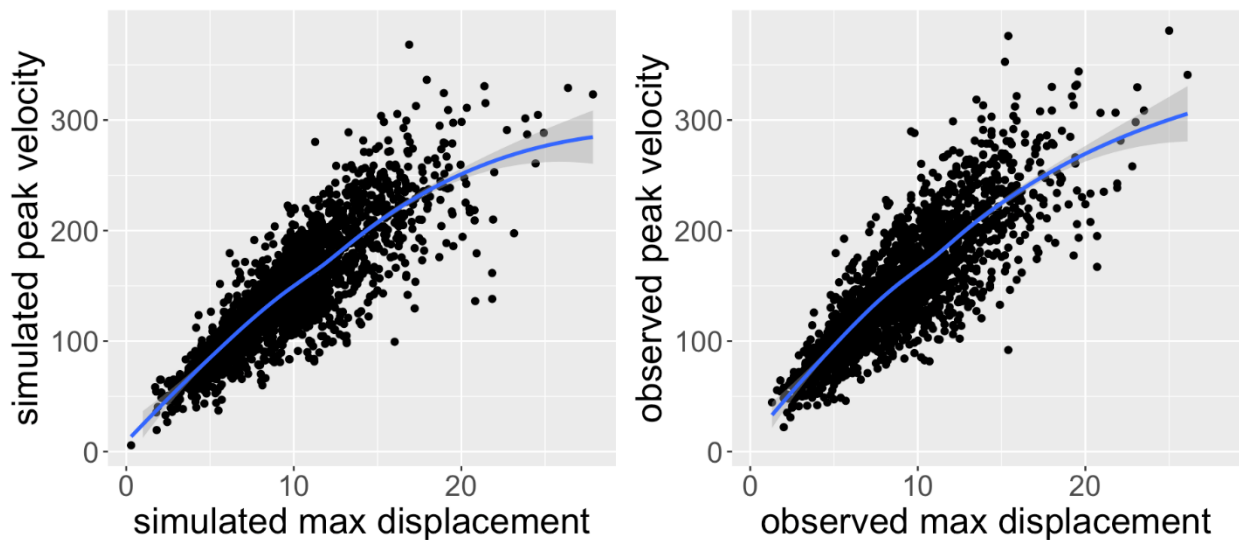


Figure 12: Relationship between maximum displacement and peak velocity in the simulated data (left) and the observed data (right).

5. Discussion

5.1 Interpretation of control parameters

The model proposed in Section 4 provides an excellent fit to observed lip constriction trajectories, generates trajectories which are qualitatively similar to observed trajectories, and captures key kinematic properties of the trajectories. The model achieves these empirical successes despite having only two control parameters: T , controlling the position of the target, and r , controlling the rapidity of the movement. The model thus has fewer parameters than the damped mass-spring model, as well as related models using time-

dependent activation (Byrd & Saltzman, 1998; Kröger et al., 1995) and cubic nonlinearity (Sorensen & Gafos, 2016). Fewer parameters means that each parameter is more clearly interpretable, allowing a clearer link to linguistically relevant dimensions. For the lip aperture (LA) trajectories examined here, T corresponds to the phonological dimension of constriction degree (CD: Browman & Goldstein, 1989) or manner of articulation, which distinguishes stops (small CD), fricatives (intermediate CD), and sonorants (large CD). For other kinds of movements, e.g., lingual movements, T may also correspond to constriction location (CL) or place of articulation. Conceptualizing T as a parameter of phonological control offers a way to concretely implement different theoretical approaches to phonological targets. In the present study, we held T constant at a single value for the duration of each movement. This is consistent with the notion that phonological targets are stable and invariant (e.g., Browman & Goldstein, 1989), in contrast to the time-varying articulatory trajectories which they contribute to. However, it would also be straightforward to select each T value from a “convex region”, as in the DIVA model (Guenther, 1995), or from a distribution of probability or activation, as in exemplar theory (Pierrehumbert, 2001) or Dynamic Field Theory (DFT: Roon & Gafos, 2016; Schöner et al., 2016). In particular, if T is selected from a neural field, as in DFT, this would allow T to vary over the course of a single movement, since neural fields are themselves dynamic.

The other control parameter, r , corresponds to the speed or rapidity of movement. This dimension is often utilized to express prosodic information. For example, movements are generally slower at phrase boundaries (Byrd & Saltzman, 1998, 2003; Cho, 2016) and they are longer in duration when part of informationally prominent words (Katsika & Tsai, 2021; Liu et al., 2023; Roessig et al., 2019; Roessig & Mücke, 2019). In some languages, temporal properties of articulatory movements can also signal lexical information through consonant gemination and vowel length. Finally, there is evidence that movement speed is manipulated to control the degree of coarticulation between overlapping movements (Du et al., 2023; Du & Gafos, 2023; Roon et al., 2021; Shaw & Chen, 2019), which has been argued to be language-specific and thus part of the learned phonological system (Shaw, 2022). Along the lines of the discussion above regarding the parameter T , conceptualizing r as a dimension of phonological control has the potential to shed light on questions about the nature of articulatory timing. Are timing goals single stable values, as is generally the case in Articulatory Phonology (AP), or are they more flexible, like the “windows” of Keating (1990)? A promising possibility is that r is generated from a dynamic neural field under the simultaneous influence of multiple linguistic forces. Under this possibility, phonological representations (as field input distributions) are stable, while the r value for any given movement is the product of multiple input distributions—relating to phonology, prosody, and inter-movement coordination—interacting in the same neural field under the additional influence of stochastic noise (e.g., Shaw & Tang, 2023).

We proposed that T generally corresponds to the phonological dimensions of place and manner of articulation (or constriction location and constriction degree) while r corresponds to phonological dimensions of gemination and length, as well as prosodic dimensions like phrase boundaries and informational prominence. However, it is not necessarily the case that the phonological dimensions indexed by each control parameter are so clearly separable. Another possibility is that a single phonological dimension can be indexed through an interaction of the two control parameters. For instance, linguistic prosody can modulate both spatial and temporal aspects of articulatory movements (Byrd & Saltzman, 1998, 2003; Katsika et al., 2014; Roessig et al., 2019; Roessig & Mücke, 2019). Under this possibility, we might expect systematic covariation between r and T . As a first-pass investigation of this issue, Figure 13 displays the relationship between the fitted r and T values for each movement by language and vowel context.

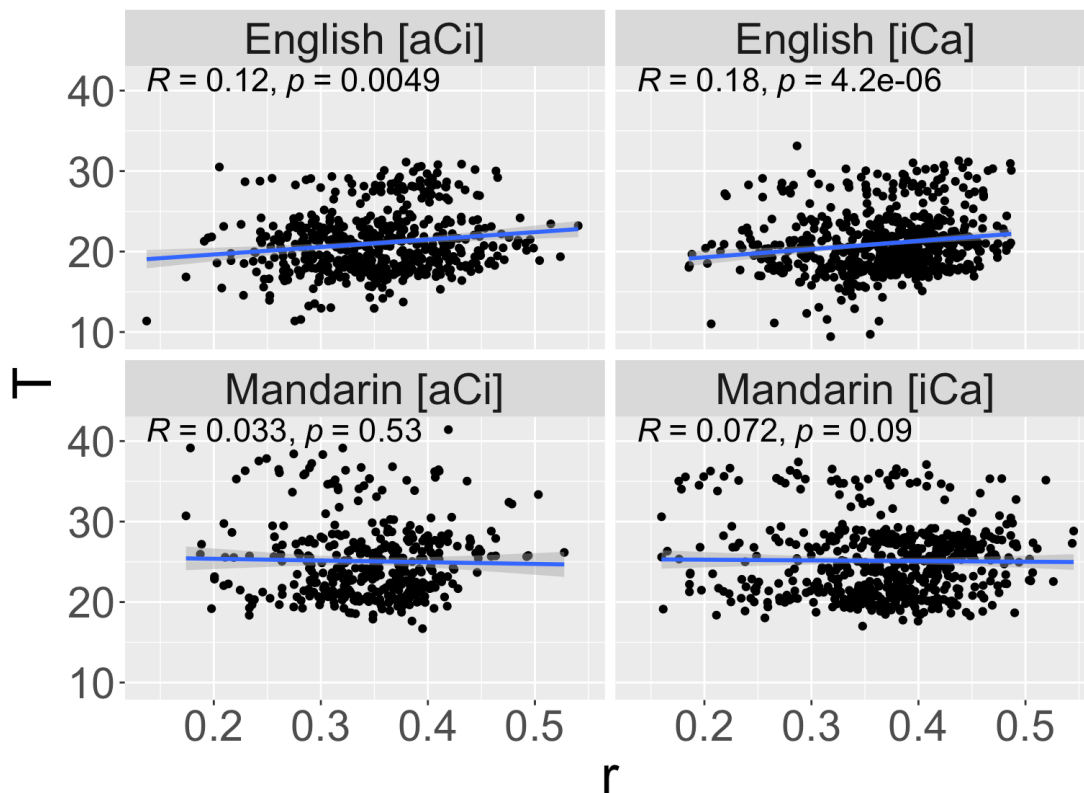


Figure 13: Relationship between fitted r and T values for each movement by language and vowel context.

There is a weak but significant positive correlation between r and T in English in both vowel contexts. In other words, movements with more extreme spatial targets (smaller T) also tend to have smaller r . Note that, for any value of r , the model generates faster movements for more extreme spatial displacements (see, e.g., Figure 12). The small positive correlation between r and T in English can be seen as mitigating this

relationship: given an extreme spatial target, the control system attenuates speed (smaller r) relative to the speed that would have been produced under an unchanged r value. Interestingly, no such correlation was observed in Mandarin. This by-language difference is an interesting puzzle. If r and T are governed by dynamic neural fields, as discussed above, then the by-language difference can be seen as a difference in coupling between fields. In English, the two fields influence each other through coupling, while in Mandarin, the two fields are independent or uncoupled. Work on lexical semantic processing in the DFT framework has proposed that the strength of coupling between neural fields varies between individuals (Stern & Piñango, 2024). The result in Figure 13 suggests that neural field coupling may also vary at the level of speech communities. This proposal is speculative at this point. The relationship between control parameters remains a fruitful area for future work.

5.2 Model characteristics

Like the family of damped mass-spring models, the system in Eq. 5 is second-order, referencing the second derivative \ddot{x} or acceleration. It is noteworthy that, although our starting point was the first-order equation in Eq. 2, formalizing the observed temporal variation in λ led to the second-order equation in Eq. 5. It is not surprising that we arrived at a second-order description, given that the empirical shapes of velocity curves are difficult to capture with first-order dynamics, as described in Section 1. Like the original version of the damped mass-spring model (Ostry & Munhall, 1985) as well as the version with a cubic term (Sorensen & Gafos, 2016) but unlike the version with time-dependent activation (Byrd & Saltzman, 1998; Kröger et al., 1995), our model is autonomous: the control law only references the internal state of the system x and \dot{x} , without referencing an external time variable t . Moreover, our model is nonlinear. Nonlinear dynamical systems are generally more difficult to analyze than linear systems. Some nonlinear systems are *chaotic*, exhibiting sensitive dependence on initial conditions and unpredictable behavior. Thus, although our model is simple in that it has only two control parameters, each with a clear linguistically relevant interpretation, the feature of nonlinearity can be seen as a source of complexity in the model. For the range of parameter values and initial conditions examined in this paper, simulated trajectories closely matched observed trajectories. However, in future work, we plan to probe the behavior of the model under a wider range of conditions in order to determine whether the model is susceptible to chaotic behavior.

The model fits (mean $R^2 = 0.88$) are comparable to or slightly higher than reported fits of the damped mass-spring model to data (Kuberski & Gafos, 2023). However, it is difficult to directly compare the R^2 values from this study to those from Kuberski & Gafos (2023). First, the details of the fitting procedures differ: Kuberski & Gafos (2023) fixed the target parameter T at the final observed value (and the parameter m at 1), and then fit the parameters k and b , both of which affect the shape of the trajectory but not the

position of the point attractor. Moreover, the data analyzed in Kuberski & Gafos (2023) came from a syllable repetition task, different from the sentence production task in the present dataset. Finally, Kuberski & Gafos (2023) examined tongue trajectories, which are more complex in that they theoretically involve multiple task dimensions, unlike the lip aperture (LA) trajectories examined in this study. In future work, we plan to address the question of the task dimensionality of articulatory movements following the approach reported here.

While model fits are overall very good, there are a number of outlying tokens which were poorly fit, even after excluding non-monotonic trajectories ($n = 306$, 10.0%) where LA was moving away from its final state for at least one sample. Moreover, in comparing simulated trajectories to observed trajectories, the average fit of the velocity curves was relatively poor (mean $R^2 = 0.45$). Figure 14 displays the observed (solid line) and simulated (dashed line) displacement, velocity, and acceleration trajectories of a representative poorly fit token.

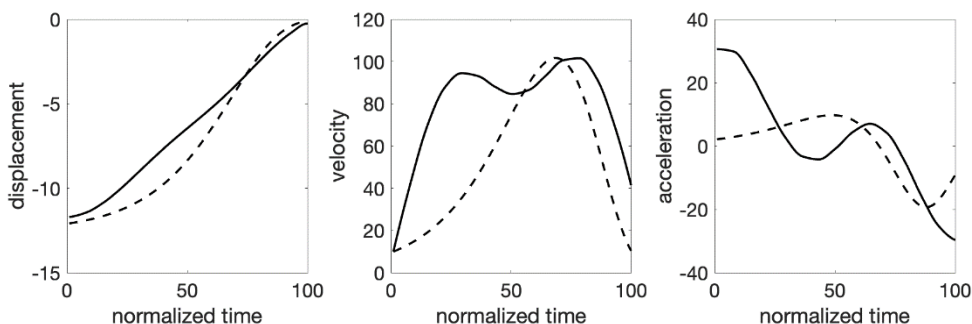


Figure 14: Observed (solid line) and simulated (dashed line) displacement (left), velocity (center), and acceleration (right) trajectories of a representative poorly fit token.

It can be seen that the magnitude of observed acceleration is initially very large, with a correspondingly steep slope in velocity. This initial rapidity then attenuates: the magnitude of velocity decreases before increasing again to another peak, and then finally decreasing again as the target is approached. In the displacement curve, this jerkiness is not particularly salient, and as a result, the model is able to match the displacement curve quite well ($R^2 = 0.89$). However, the model-generated acceleration and velocity curves are much smoother than the observed curves, leading to a worse fit for acceleration ($R^2 = 0.30$) and an extremely poor fit for velocity ($R^2 = -1.63$). In fact, in its current form, the model is unable to generate trajectories with multiple velocity peaks. This arises ultimately from our starting assumption of point attractor dynamics, formalized in Eq. 2. If this assumption is justified, then what is the source of trajectories with multiple velocity peaks, like the one in Figure 14, as well as non-monotonic state trajectories, which we excluded from analysis? One potential source is noise in the control system, e.g., stochastic influences on the neural processes governing movement parameter generation as well as muscle contraction (e.g.,

Mücke et al., 2024; Parrell et al., 2023). These “abnormal” trajectories might also suggest an influence of target-based timing (e.g., Turk & Shattuck-Hufnagel, 2020). For instance, if a movement’s target achievement is actively timed to a landmark in another movement, then the movement might slow down or even reverse direction in order to “wait for” the other movement (e.g., Kramer et al., 2023). This could be modeled with the addition of a coupling term that references the state of another movement. Eq. 5, as a proposal for the basic dynamics of individual articulatory movements, offers a starting point from which to examine additional influences on movement, like inter-movement coordination. We plan to pursue this issue in future work.

Another apparent shortcoming of the model in matching empirical trajectories is observed in the kinematic variable of relative time to peak velocity as a ratio of total movement duration (see, e.g., Figure 11). While variation in the two parameters r and T is able to capture some of the observed variation in relative time to peak velocity ($R^2 = 0.34$, $p < .001$), this R^2 value is relatively low, by far the lowest compared to the other kinematic variables examined. It is a feature of the model that relative time to peak velocity is very stable under variation in model parameter values. It is possible that the observed variability arises from factors outside of the basic dynamics of individual movements (as discussed above). Two of the three subjects analyzed in Byrd & Saltzman (1998) exhibited stability in relative time to peak velocity under variation in the strength of an adjacent prosodic boundary. However, one of their subjects exhibited systematic variability: stronger boundaries corresponded to earlier peaks. Using the damped mass-spring model with time-dependent activation, they were able to capture this variation by manipulating both stiffness k and the shape parameters of the activation curve. In future work, we plan to probe the capacity and limits of our model to account for kinematic variation conditioned by prosodic context.

As a final point, the data motivating our model comes only from labial constriction movements, which is a small subset of the movement types relevant for speech articulation. However, compared to datasets motivating other dynamical models (see Table 1), this dataset is relatively large and diverse: 2110 tokens of meaningful speech in multiple prosodic contexts from 24 speakers of two unrelated languages. Thus, while we should be cautious at this point in generalizing these findings to other kinds of movements, the empirical support for the patterns uncovered regarding these movements is relatively strong.

6. Conclusion

We discovered that the ratio of instantaneous displacement, $-x + T$, to instantaneous velocity, \dot{x} , decays exponentially over the course of labial constriction movements for /b/ and /m/ in English and Mandarin. Formalizing this discovery led to the derivation of an autonomous, nonlinear, second-order dynamical

model of speech articulatory movements. The model achieves excellent fits to empirical trajectories with only two control parameters, T and r . T controls the position of the target, and r controls the rapidity of the movement. These parameters, by hypothesis, are under cognitive control and constitute dimensions of phonological contrast in language. As a basic dynamical model of the control of individual articulatory movements, it offers a starting point from which to understand additional influences on movement, like prosody, inter-movement coordination, and stochastic noise in motor control.

7. References

- Abbs, J. H., & Gracco, V. L. (1984). Control of complex motor gestures: Orofacial muscle responses to load perturbations of lip during speech. *Journal of Neurophysiology*, *51*(4), 705–723. <https://doi.org/10.1152/jn.1984.51.4.705>
- Browman, C. P., & Goldstein, L. (1989). Articulatory gestures as phonological units. *Phonology*, *6*(2), 201–251. <https://doi.org/10.1017/S0952675700001019>
- Brunton, S. L., Proctor, J. L., & Kutz, J. N. (2016). Discovering governing equations from data by sparse identification of nonlinear dynamical systems. *Proceedings of the National Academy of Sciences*, *113*(15), 3932–3937. <https://doi.org/10.1073/pnas.1517384113>
- Byrd, D., & Saltzman, E. (1998). Intragestural dynamics of multiple prosodic boundaries. *Journal of Phonetics*, *26*(2), 173–199. <https://doi.org/10.1006/jpho.1998.0071>
- Byrd, D., & Saltzman, E. (2003). The elastic phrase: Modeling the dynamics of boundary-adjacent lengthening. *Journal of Phonetics*, *31*(2), 149–180. [https://doi.org/10.1016/S0095-4470\(02\)00085-2](https://doi.org/10.1016/S0095-4470(02)00085-2)
- Cho, T. (2016). Prosodic Boundary Strengthening in the Phonetics–Prosody Interface. *Language and Linguistics Compass*, *10*(3), 120–141. <https://doi.org/10.1111/lnc3.12178>
- Cooke, J. D. (1980). The Organization of Simple, Skilled Movements. In G. E. Stelmach & J. Requin (Eds.), *Advances in Psychology* (pp. 199–212). North-Holland. [https://doi.org/10.1016/S0166-4115\(08\)61946-9](https://doi.org/10.1016/S0166-4115(08)61946-9)

- Du, S., & Gafos, A. I. (2023). Articulatory overlap as a function of stiffness in German, English and Spanish word-initial stop-lateral clusters. *Laboratory Phonology*, 14(1), Article 1.
<https://doi.org/10.16995/labphon.7965>
- Du, S., Kuberski, S., & Gafos, A. I. (2023). How measures of gestural overlap relate to dynamics: Evidence from German and English word-initial stop-lateral clusters. *Proceedings of the 20th International Congress of Phonetic Sciences (ICPhS)*, 2164–2168.
- Elie, B., Lee, D. N., & Turk, A. (2023). Modeling trajectories of human speech articulators using general Tau theory. *Speech Communication*, 151, 24–38. <https://doi.org/10.1016/j.specom.2023.04.004>
- Elie, B., Šimko, J., & Turk, A. (2024). Optimization-based planning of speech articulation using general Tau Theory. *Speech Communication*, 160, 103083. <https://doi.org/10.1016/j.specom.2024.103083>
- Fowler, C. A. (1980). Coarticulation and theories of extrinsic timing. *Journal of Phonetics*, 8, 113–133.
- Garcia, D. (2010). Robust smoothing of gridded data in one and higher dimensions with missing values. *Computational Statistics and Data Analysis*, 54(4), 1167–1178.
<https://doi.org/10.1016/j.csda.2009.09.020>
- Guenther, F. H. (1995). Speech sound acquisition, coarticulation, and rate effects in a neural network model of speech production. *Psychological Review*, 102(3), 594–621.
<https://doi.org/10.1037/0033-295X.102.3.594>
- Iskarous, K. (2017). The relation between the continuous and the discrete: A note on the first principles of speech dynamics. *Journal of Phonetics*, 64, 8–20. <https://doi.org/10.1016/j.wocn.2017.05.003>
- Iskarous, K., & Pouplier, M. (2022). Advancements of phonetics in the 21st century: A critical appraisal of time and space in Articulatory Phonology. *Journal of Phonetics*, 95, 101195.
<https://doi.org/10.1016/j.wocn.2022.101195>
- Katsika, A., Krivokapić, J., Mooshammer, C., Tiede, M., & Goldstein, L. (2014). The coordination of boundary tones and its interaction with prominence. *Journal of Phonetics*, 44(1), 62–82.
<https://doi.org/10.1016/j.wocn.2014.03.003>

- Katsika, A., & Tsai, K. (2021). The supralaryngeal articulation of stress and accent in Greek. *Journal of Phonetics*, 88, 101085. <https://doi.org/10.1016/j.wocn.2021.101085>
- Keating, P. A. (1990). The window model of coarticulation: Articulatory evidence. In M. E. Beckman & J. Kingston (Eds.), *Papers in Laboratory Phonology I: Between the Grammar and the Physics of Speech* (pp. 451–470). Cambridge University Press.
- Kramer, B. M., Stern, M. C., Wang, Y., Liu, Y., & Shaw, J. A. (2023). Synchrony and stability of articulatory landmarks in English and Mandarin CV sequences. *Proceedings of the 20th International Congress of Phonetic Sciences (ICPhS)*, 1022–1026.
- Kröger, B. J., Schröder, G., & Opgen-Rhein, C. (1995). A gesture-based dynamic model describing articulatory movement data. *The Journal of the Acoustical Society of America*, 98(4), 1878–1889. <https://doi.org/10.1121/1.413374>
- Kuberski, S. R., & Gafos, A. I. (2023). How thresholding in segmentation affects the regression performance of the linear model. *JASA Express Letters*, 3(9), 095202. <https://doi.org/10.1121/10.0020815>
- Lee, D. N. (1998). Guiding Movement by Coupling Taus. *Ecological Psychology*, 10(3–4), 221–250. <https://doi.org/10.1080/10407413.1998.9652683>
- Lindblom, B. (1963). Spectrographic Study of Vowel Reduction. *The Journal of the Acoustical Society of America*, 35(5), 783–783. <https://doi.org/10.1121/1.2142410>
- Liu, Y., Wang, Y., Stern, M. C., Kramer, B. M., & Shaw, J. A. (2023). Temporal scope of articulatory slowdown under informational focus: Data from English and Mandarin. *Proceedings of the 20th International Congress of Phonetic Sciences*, 1691–1695.
- Moon, S., & Lindblom, B. (1994). Interaction between duration, context, and speaking style in English stressed vowels. *The Journal of the Acoustical Society of America*, 96(1), 40–55. <https://doi.org/10.1121/1.410492>

- Mücke, D., Roessig, S., Thies, T., Hermes, A., & Mefferd, A. (2024). Challenges with the kinematic analysis of neurotypical and impaired speech: Measures and models. *Journal of Phonetics*, *102*, 101292. <https://doi.org/10.1016/j.wocn.2023.101292>
- Ostry, D. J., Cooke, J. D., & Munhall, K. G. (1987). Velocity curves of human arm and speech movements. *Experimental Brain Research*, *68*(1), 37–46. <https://doi.org/10.1007/BF00255232>
- Ostry, D. J., & Munhall, K. G. (1985). Control of rate and duration of speech movements. *The Journal of the Acoustical Society of America*, *77*(2), 640–648. <https://doi.org/10.1121/1.391882>
- Parrell, B. (2011). Dynamical account of how /b, d, g/ differ from /p, t, k/ in Spanish: Evidence from labials. *Laboratory Phonology*, *2*(2), 423–449. <https://doi.org/10.1515/labphon.2011.016>
- Parrell, B., Mefferd, A., Harper, S., Roessig, S., & Mücke, D. (2023). Using computational models to characterize the role of motor noise in speech: The case of amyotrophic lateral sclerosis. *Proceedings of the 20th International Congress of Phonetic Sciences*, 878–882.
- Perrier, P., Abry, C., & Keller, E. (1988). Vers une modélisation des mouvements du dos de la langue. *Vers Une Modélisation Des Mouvements Du Dos de La Langue*, *2–1*, 45–63.
- Pierrehumbert, J. B. (2001). Exemplar dynamics: Word frequency, lenition and contrast. In J. Bybee & P. J. Hopper (Eds.), *Frequency and the Emergence of Linguistic Structure* (pp. 137–158). John Benjamins.
- R Core Team. (2021). *R: A language and environment for statistical computing*. [Computer software]. R Foundation for Statistical Computing.
- Roessig, S., & Mücke, D. (2019). Modeling Dimensions of Prosodic Prominence. *Frontiers in Communication*, *4*(September), 1–19. <https://doi.org/10.3389/fcomm.2019.00044>
- Roessig, S., Mücke, D., & Grice, M. (2019). The dynamics of intonation: Categorical and continuous variation in an attractor-based model. *PLoS ONE*, *14*(5). <https://doi.org/10.1371/journal.pone.0216859>

- Roon, K. D., & Gafos, A. I. (2016). Perceiving while producing: Modeling the dynamics of phonological planning. *Journal of Memory and Language*, 89, 222–243.
<https://doi.org/10.1016/j.jml.2016.01.005>
- Roon, K. D., Hoole, P., Zeroual, C., Du, S., & Gafos, A. I. (2021). Stiffness and articulatory overlap in Moroccan Arabic consonant clusters. *Laboratory Phonology: Journal of the Association for Laboratory Phonology*, 12(1), 8. <https://doi.org/10.5334/labphon.272>
- Saltzman, E. L., & Munhall, K. G. (1989). A Dynamical Approach to Gestural Patterning in Speech Production. *Ecological Psychology*, 1(4), 333–382.
- Schöner, G., Spencer, J., & Group, D. R. (2016). *Dynamic Thinking: A Primer on Dynamic Field Theory*. Oxford University Press.
- Shaw, J. A. (2022). Micro-prosody. *Language and Linguistics Compass*, 16(2), 1–21.
<https://doi.org/10.1111/lnc3.12449>
- Shaw, J. A., & Chen, W. (2019). Spatially Conditioned Speech Timing: Evidence and Implications. *Frontiers in Psychology*, 10, 1–17. <https://doi.org/10.3389/fpsyg.2019.02726>
- Shaw, J. A., & Tang, K. (2023). A dynamic neural field model of leaky prosody: Proof of concept. *Proceedings of the 2022 Annual Meeting on Phonology (AMP)*.
<https://doi.org/10.3765/amp.v10i0.5442>
- Sorensen, T., & Gafos, A. (2016). The Gesture as an Autonomous Nonlinear Dynamical System. *Ecological Psychology*, 28(4), 188–215. <https://doi.org/10.1080/10407413.2016.1230368>
- Stern, M. C., & Piñango, M. M. (2024). *Contextual modulation of language comprehension in a dynamic neural model of lexical meaning* (arXiv:2407.14701). arXiv.
<https://doi.org/10.48550/arXiv.2407.14701>
- Tiede, M. (2005). *MVIEW: Software for visualization and analysis of concurrently recorded movement data* [Computer software]. Haskins Laboratories.
- Turk, A., & Shattuck-Hufnagel, S. (2020). *Speech Timing: Implications for Theories of Phonology, Phonetics, and Speech Motor Control*. Oxford University Press.

van Gelder, T. (1998). The dynamical hypothesis in cognitive science. *Behavioral and Brain Sciences*,
21(5), 615–628. <https://doi.org/10.1017/S0140525X98001733>

7. Appendix A: Derivation of second-order differential equation (Eq. 5)

$$\frac{d}{dt}((-x + T)/\dot{x}) = -r * (-x + T)/\dot{x} \quad \text{(i) substitution}$$

$$(-x + T) * \frac{d}{dt}(1/\dot{x}) + (1/\dot{x}) * \frac{d}{dt}(-x + T) = -r * (-x + T)/\dot{x} \quad \text{(ii) product rule}$$

$$(-x + T) * (-1/\dot{x}^2) * \ddot{x} + (1/\dot{x}) * \frac{d}{dt}(-x + T) = -r * (-x + T)/\dot{x} \quad \text{(iii) chain rule, power rule}$$

$$(-x + T) * (-1/\dot{x}^2) * \ddot{x} + (1/\dot{x}) * \left(-\dot{x} + \frac{dT}{dt}\right) = -r * (-x + T)/\dot{x} \quad \text{(iv) sum rule}$$

$$(-x + T) * (-1/\dot{x}^2) * \ddot{x} - 1 = -r * (-x + T)/\dot{x} \quad \text{(v) } \frac{dT}{dt} = 0$$

$$-\ddot{x}(-x + T)/\dot{x}^2 = -r * (-x + T)/\dot{x} + 1 \quad \text{(vi) simplification}$$

$$-\ddot{x}(-x + T) = -r\dot{x} * (-x + T) + \dot{x}^2 \quad \text{(vii) simplification}$$

$$\ddot{x} = r\dot{x} - \dot{x}^2/(-x + T) \quad \text{(viii) simplification}$$